



Synergistic effect of electron-transfer mediator and interfacial catalytic active-site for the enhanced H₂-evolution performance: A case study of CdS-Au photocatalyst

Ping Wang^a, Yue Sheng^a, Fazhou Wang^b, Huogen Yu^{a,b,*}

^a Department of Chemistry, School of Chemistry, Chemical Engineering and Life Sciences, Wuhan University of Technology, Wuhan 430070, People's Republic of China

^b State Key Laboratory of Silicate Materials for Architectures, Wuhan University of Technology, Wuhan 430070, People's Republic of China



ARTICLE INFO

Keywords:
Photocatalysis
H₂ evolution
Synergistic effect
CdS
Cocatalyst

ABSTRACT

For noble metal cocatalyst-modified photocatalysts with a high H₂-evolution performance, both of the rapid electron transfer (or electron capture) from semiconductor to cocatalyst and the following interfacial catalysis for H₂ production on the cocatalyst surface are highly required. Compared with Pt-loaded photocatalyst, Au-modified sample usually shows an obviously lower H₂-evolution activity due to its inefficient H₂-production rate on the Au cocatalyst surface. In this study, the SCN[−] ions as the catalytic active sites are selectively adsorbed on the Au surface of CdS/Au photocatalysts (CdS/Au-SCN), with the aim of promoting the interfacial H₂-evolution reaction on Au cocatalyst and improving the photocatalytic water-splitting efficiency of CdS/Au system. The CdS/Au-SCN photocatalysts were synthesized via a two-step process including the initial photoinduced deposition of Au nanoparticles on CdS surface and the following selective adsorption of SCN[−] on the Au surface by an impregnation method. It was found that the resultant CdS/Au-SCN photocatalysts exhibited obviously improved photocatalytic H₂-evolution activity compared with the CdS, CdS/Au and CdS/SCN photocatalysts. Especially, the CdS/Au-SCN(0.5 mM) achieved the highest photocatalytic activity (109.60 μmol h^{−1}) with an apparent quantum efficiency (QE) of 11.25%, which was clearly higher than that of CdS and CdS/Au by a factor of 2.3 and 1.5 times, respectively. The enhanced H₂-evolution performance of CdS/Au-SCN can be attributed to the excellent synergistic effect of Au and SCN[−], namely, the Au nanoparticle functions as an effective electron-transfer mediator for the steady capture and rapid transportation of photogenerated electrons from CdS surface, while the adsorbed SCN[−] serves as the interfacial catalytic active-site to effectively adsorb H⁺ ions from solution and promote the rapid H₂-evolution reaction. The present synergistic mechanism of electron-transfer mediator and interfacial catalytic active-sites may provide some new insights for the design of highly efficient photocatalytic materials.

1. Introduction

Photocatalytic H₂-evolution from water splitting based on semiconductor has been regarded as one of the most potential solutions to resolve the serious energy crisis [1–6]. Among various semiconductor materials, CdS serves as one of the most competitive photocatalysts owing to its appropriate band gap (2.4 eV) and strong reduction potential (−0.51 V vs. SHE) for H₂-evolution [7–10]. Unfortunately, pure CdS usually exhibits a limited photocatalytic H₂-evolution performance owing to the rapid recombination of photogenerated electron-hole pairs in the bulk or on its surface [11,12] (Fig. 1a). To improve the photocatalytic H₂-evolution performance of CdS, one of the effective

strategies is loading noble-metal nanoparticles as the effective electron cocatalysts (such as Pt [13,14] and Pd [15,16]) to promote the separation efficiency of photogenerated charges. In this case, metallic Pt is one of the most well-known and highly effective electron-cocatalysts for the enhanced H₂-evolution activity of CdS due to its excellent catalytic activity for interfacial H₂ evolution [17] (Fig. 1b). However, in addition to its high cost, Pt cocatalysts usually can become the recombination active sites for the back reaction of produced H₂ and O₂ [18], causing a decreased H₂-evolution performance. Compared with metallic Pt with a high work function of 5.7 eV [19], the Au cocatalyst with smaller work function of 5.1 eV [20] not only shows less active for the back reaction of H₂ and O₂ [21], but also possesses an obviously

* Corresponding author at: Department of Chemistry, School of Chemistry, Chemical Engineering and Life Sciences, Wuhan University of Technology, Wuhan 430070, People's Republic of China.

E-mail address: yuhogen@whut.edu.cn (H. Yu).

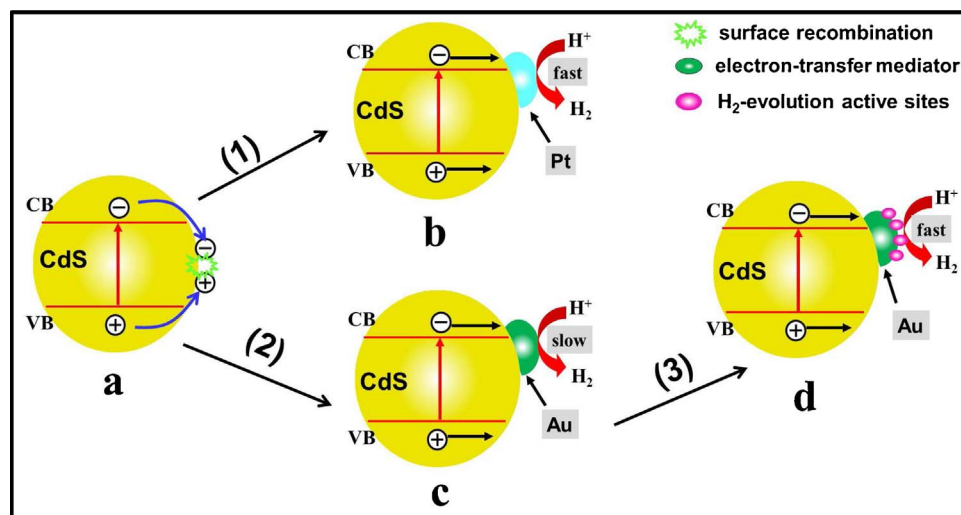


Fig. 1. Schematic drawing illustrating the strategies to develop highly efficient CdS photocatalysts: (1) Pt modification; (2) Au modification; (3) coupling modification of Au and interface catalytic active sites.

lower cost. As a consequence, the noble metallic Au can work as a competitive electron cocatalyst to boost up the photocatalytic H₂-evolution performance of various photocatalysts. However, the present H₂-evolution efficiency of Au-modified CdS (CdS/Au) is obviously lower than that of Pt/CdS photocatalysts [20,22]. Therefore, it is highly essential and worthwhile to develop new strategy to further improve the photocatalytic H₂-evolution performance of CdS/Au photocatalysts.

To achieve a high H₂-evolution performance for cocatalyst-modified photocatalysts, both of the rapid electron transfer (or electron capture) from semiconductor to cocatalyst and the efficient interfacial catalysis for H₂ production on the cocatalyst surface are highly required [23]. In this case, the electron cocatalysts not only work as the electron-transfer mediator to rapidly capture photogenerated electrons, but also act as the catalytic active sites for the effective interfacial reaction. Thus, various high-performance cocatalyst-modified photocatalytic materials, mainly dual cocatalyst-modified photocatalysts, have been widely developed via the synergistic effect of rapid electron transfer and efficient interfacial catalysis [24–27]. For example, Lv et al. [28] proved that the simultaneous loading of graphene (as an electron acceptor) and Cu nano-clusters (as active sites) could improve the photocatalytic H₂-evolution performance of TiO₂. Xiang et al. [29] found that TiO₂ nanoparticles showed enhanced H₂-evolution activity by loading graphene as an electron collector and MoS₂ nanosheets as active sites. In addition, Jia et al. [30] reported that the H₂-evolution performance of CdS photocatalyst was greatly improved by the introduction of graphene (as an electron mediator) and MoS₂ nanoplates. In our recent work, we also demonstrated that dual electron-cocatalyst-modified TiO₂ photocatalysts with rGO as an electron-transfer mediator and Fe(III) as oxygen-reduction active-sites exhibited obviously improved photocatalytic activity [31]. Clearly, the above reports strongly demonstrated a general and very effective strategy to improve the photocatalytic performance of various photocatalysts, namely, the simultaneous loading of electron-transfer mediator (such as reduced graphene oxide) and interfacial catalytic-active sites (such as Cu nano-clusters, Fe(III), and MoS₂) due to their excellent synergistic effect. For the Au-modified CdS photocatalyst, only a limited improvement of H₂-evolution performance can be found compared with the bare CdS. In fact, compared with Pt cocatalyst with a rapid discharge of photogenerated electrons from its surface to surrounding medium (such as H⁺), Au catalyst usually can store captured electrons from semiconductors surface and exhibits a capacitive property, resulting in a slow interfacial catalytic reaction for H₂ evolution [32,33] (Fig. 1c). Therefore, on the basis of the above analysis, it is expected that the photocatalytic H₂-evolution performance of CdS/Au can be greatly improved by loading effective catalytic active-sites on the Au surface

(Fig. 1d).

More recently, it was found that the adsorption of SCN[−] ions on Ag facilitates the transfer of photogenerated electrons on the Ag/TiO₂ electrode, resulting in improved photocatalytic H₂-evolution performance of Ag/TiO₂ [34]. Considering a strong affinity between Au and sulfur compounds (such as SCN[−] ions), it is expected that the selective modification of SCN[−] ions on the Au surface can obviously improve the photocatalytic performance of CdS/Au due to the possible synergistic effect of Au as an electron-transfer mediator and SCN[−] as the interfacial catalytic active-sites. In this study, highly efficient CdS photocatalysts co-modified by Au as electron-transfer mediator and SCN[−] as interfacial catalytic active-sites (referred to as CdS/Au-SCN) were synthesized via a two-step process including the initial photoinduced deposition of Au on the CdS surface and the following selective loading of SCN[−] on the Au surface by an impregnation method. It was found that the CdS/Au-SCN photocatalyst exhibited excellent photocatalytic H₂-evolution activity compared with the bare CdS, CdS/Au and CdS/SCN. On the basis of the experimental results, a synergistic effect mechanism of Au and SCN[−] was proposed to account for its improved photocatalytic performance. To the best of our knowledge, this is the first report about the selective adsorption of SCN[−] on the Au cocatalyst surface to greatly improve the photocatalytic H₂-evolution performance of CdS/Au. This work may provide some new insights for the smart design and development of highly efficient photocatalytic materials for various potential applications.

2. Experimental section

2.1. Preparation of CdS sample

CdS sample was synthesized by a frequently-used precipitation method. In brief, 140 mL of 0.1 mol L^{−1} Na₂S solution was added dropwise into 140 mL of 0.1 mol L^{−1} Cd(NO₃)₂ solution. The resulting suspension was vigorously stirred at room temperature for 2 h and then it was allowed to stay for overnight. The orange-red precipitate was collected by filtration, rinsed with plenty of deionized water, and dried at 60 °C for 24 h. After the product was ground into powder, the resulting product was calcined at 550 °C for 4 h under a nitrogen gas flow.

2.2. Preparation of CdS/Au photocatalysts

The Au-modified CdS photocatalyst (CdS/Au) was prepared via a typical photodeposition method. First, 50 mg of CdS powder was dispersed in 80 mL of aqueous solution containing 0.35 mol L^{−1} of Na₂S and 0.25 mol L^{−1} of Na₂SO₃ as sacrificial agents. Second, 76 μL of

HAuCl_4 solution (0.1 mol L^{-1}) was injected into the above suspension quickly, and the system was then bubbled with nitrogen for 15 min to remove the dissolved oxygen. Third, Au nanoparticles were loaded on the CdS surface through a photodeposition process by visible-light irradiation (350 W xenon lamp) for 30 min (in this case, the resultant CdS/Au suspension was also used as the precursor to prepare the following CdS/Au-SCN photocatalysts, and the details are shown in Section 2.3). Finally, the products were collected by filtration, flushed several times with deionized water and dried at 60°C for 24 h to obtain the CdS/Au photocatalyst. In this study, the amount of Au to CdS was controlled to be 3 wt%, and the resultant CdS/Au (3 wt%) sample was referred to as CdS/Au.

2.3. Preparation of CdS/Au-SCN photocatalysts

The selective modification of SCN^- ions on the Au nanoparticles could be prepared via an impregnation method by using above CdS/Au suspension (Section 2.2) as the precursor, and the resultant samples were referred to as CdS/Au-SCN photocatalysts. Typically, a calculated amount of 0.1 mol L^{-1} potassium thiocyanate (KSCN) solution was injected into the above CdS/Au suspension. To prevent the possible oxidation of thiocyanate, the whole process was conducted under N_2 atmosphere. After stirring at ambient temperature for 1 h with the aiming of completely selective adsorption for SCN^- ions on the Au surface, the resultant suspension was harvested by filtration, rinsed with deionized water, and finally dried at 60°C to obtain the CdS/Au-SCN photocatalysts. To investigate the effect of thiocyanate amount on the photocatalytic performance of CdS/Au photocatalyst, the thiocyanate concentration was controlled to be 0, 0.1, 0.5 and 5 mmol L^{-1} , and the resulting corresponding samples were denoted as CdS/Au, CdS/Au-SCN(0.1 mM), CdS/Au-SCN(0.5 mM), and CdS/Au-SCN(5 mM), respectively. For comparison, SCN^- -modified CdS photocatalyst (CdS/SCN) was also prepared by an identical experimental method with a thiocyanate concentration of 0.5 mmol L^{-1} .

2.4. Characterization

X-ray powder diffraction was used to identify the crystal structures and phase compositions of the samples. Diffraction data were obtained on a Rigaku Ultima III X-ray Diffractometer (Japan) using $\text{Cu K}\alpha$ radiation source. Morphological observations were conducted on a JSM-7500 field emission scanning electron microscope (FESEM, JEOL, Japan) equipped with an X-Max 50 energy-dispersive X-ray spectrometer (EDX, Oxford Instruments, UK) and a JEM-2100F transmission electron microscope (TEM, JEOL, Japan). UV-vis absorption spectra were obtained using a UV-vis spectrophotometer (UV-2450, Shimadzu, Japan). BaSO_4 was used as a reflectance standard in a UV-vis diffuse reflectance experiment. X-ray photoelectron spectroscopy (XPS) measurements were done on a KRATOA XSAM800 XPS system (UK) with Al $\text{K}\alpha$ source. All the binding energies were referenced to the C1s peak at 284.6 eV for the surface adventitious carbon.

2.5. Photocatalytic H_2 -evolution activity

The photocatalytic H_2 -evolution experiments were conducted in a 100 mL three-necked Pyrex flask at ambient temperature and atmospheric pressure, and the outlets of the flask were sealed with a silicone rubber septum. A 350-W xenon lamp with a UV cutoff filter ($\lambda \geq 420 \text{ nm}$), which was positioned 20-cm away from the reactor, served as the irradiation light source to trigger the photocatalytic reaction. The focused intensity on the flask was about 180 mW cm^{-2} , which was measured by a FZ-A visible-light radiometer (made in photoelectric instrument factory of Beijing Normal University, China). In a typical experiment, 50 mg of photocatalyst was dispersed in 80 mL of aqueous solution containing 0.35 mol L^{-1} Na_2S and 0.25 mol L^{-1} Na_2SO_3 . The system was bubbled with nitrogen for 15 min to remove

the dissolved oxygen. In the process of irradiation, continuous stirring was applied to keep the photocatalyst particles in suspension state. Gas (0.4 mL) was intermittently sampled through a septum, and hydrogen was analyzed by a gas chromatograph (Shimadzu GC-2014C, Japan, with nitrogen as a carrier gas) equipped with a 5 \AA molecular sieve column and a thermal conductivity detector. The QE was calculated by using the following equation

$$\begin{aligned} \text{QE}(\%) &= \frac{\text{number of reacted electrons}}{\text{number of incident photons}} \times 100 \\ &= \frac{\text{number of evolved } \text{H}_2 \text{ molecules} \times 2}{\text{number of incident photons}} \times 100 \end{aligned}$$

2.6. Photoelectrochemical measurements

Photoelectrochemical measurements were performed on an electrochemical workstation (CHI660E, China) in a standard three-electrode configuration in 0.5 mol L^{-1} Na_2SO_4 electrolyte solution [35,36]. In the system, platinum wire is the counter electrode and a standard Ag/AgCl electrode is the reference electrode. High-purity N_2 was purged into the three-electrode cell for 15 min to remove O_2 before all the testing. The light source was provided by one 3-W LED (420-nm light source with a 90-mW cm^{-2} power). The working electrodes were spread on fluorine-doped tin oxide (FTO) conductor glass substrate with an active area of about 1.0 cm^2 . Typically, the sample (10 mg) was dispersed into the ethanol-Nafion solution (1 mL of anhydrous ethanol and 1 mL of D-520 Nafion (5%, w/w, in water and 1-propanol, Alfa Aesar)), and then ultrasonicated for 30 min to obtain the suspension solution. The suspension was spread on the FTO glass with the side protected by Scotch tape. After air drying, the working electrode was further dried at 60°C for 1 h. Finally, linear sweep voltammetry (LSV) curves were measured at the potential ranging from -0.1 to -0.5 V with a scan rate of 10 mV s^{-1} and the transient photocurrent responses with time ($i-t$ curve) of the working electrodes were measured at a -0.2 V bias potential during repeated ON/OFF illumination cycles. For the incident photon-to-electron conversion efficiency (IPCE) measurement, several 3-W LED lights with different wavelengths were used as light sources. The percent IPCE at λ , %IPCE(λ), was calculated by the following equation [37]:

$$\% \text{IPCE}(\lambda) = 1240 \times \frac{J(\lambda)}{\lambda^* I_0(\lambda)} \times 100$$

where λ is the wavelength of light (nm), $J(\lambda)$ is the photocurrent density (mA cm^{-2}) under illumination at λ , and $I_0(\lambda)$ is the incident-light intensity (mW m^{-2}) at λ .

Differential pulse voltammetry (DPV) measurements were performed on an electrochemical workstation (CHI660E) in a standard three-electrode configuration in a 5.0 mmol L^{-1} $[\text{Fe}(\text{CN})_6]^{3-/-4-}$ solution [38,39] in a potential scanning range from -0.3 V to $+0.6 \text{ V}$ with a scan rate of 100 mV s^{-1} . In this case, the Au-loaded glassy carbon electrode (GCE/Au) and SCN^- -modified GCE/Au (GCE/Au-SCN) were first prepared. For details, Au nanoparticles were electrochemical deposited on the highly polished GCE surface to form GCE/Au under cyclic voltammetry scanning from -0.6 to $+1.5 \text{ V}$ with a scan rate of 100 mV s^{-1} for 25 cycles in 0.01 mmol L^{-1} HAuCl_4 solution, while the GCE/Au-SCN was accomplished via soaking the above GCE/Au in the 0.1 mol L^{-1} KSCN solution for 1 h.

3. Results and discussion

3.1. Strategy for the facile synthesis of CdS/Au-SCN photocatalyst

The synthetic procedure of CdS/Au-SCN photocatalyst can be succinctly illustrated by a facile photoinduced deposition of Au nanoparticles and the subsequently selective impregnation of SCN^- ions on

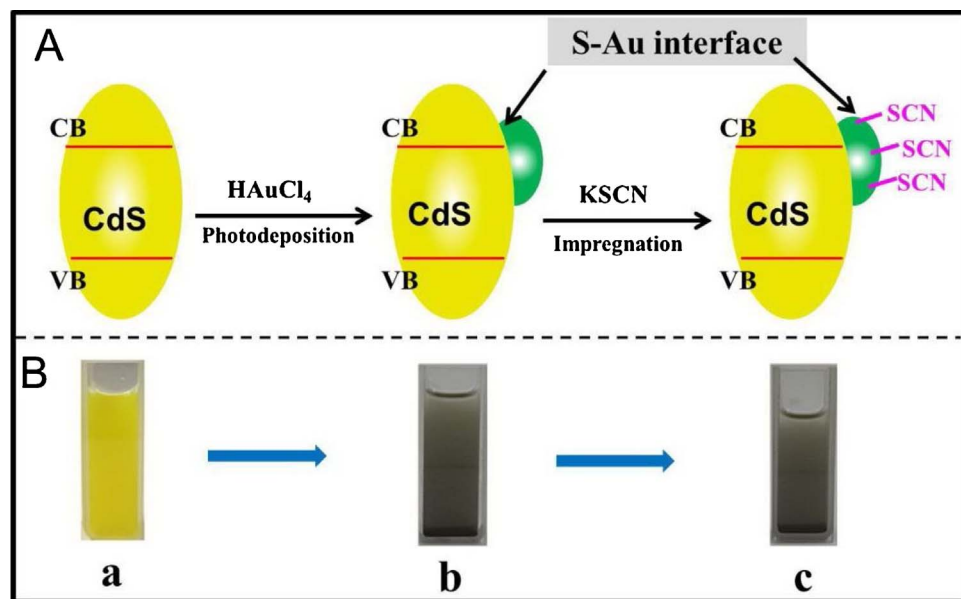


Fig. 2. Graphical illustration for the synthesis of different samples: (a) CdS, (b) CdS/Au, and (c) CdS/Au-SCN.

Au surface (Fig. 2). First, the CdS photocatalyst is prepared by a well-known high-temperature calcination method to form highly crystalline CdS particles (Fig. 2A-a). In this case, the resultant CdS sample shows a bright yellow even when dispersing into water to form suspension solution (Fig. 2B-a), in good agreement with the widely reported results [40]. For the preparation of CdS/Au sample (Fig. 2A-b), Au(III) in the HAuCl₄ solution are *in situ* reduced to form Au(0) nanoparticles and then deposited on the CdS surface via a typical photodeposition method. In this case, the color of CdS suspension solution changed obviously from bright yellow to dark (Fig. 2B-b), suggesting the successful deposition of Au nanoparticles (the dark color is caused by the localized surface plasmon resonance of Au nanoparticles). As for the formation of CdS/Au-SCN photocatalyst (Fig. 2A-c), the above CdS/Au sample was dispersed into a KSCN solution and then stirred at ambient temperature for 1 h. In this case, considering the well-known strong affinity of gold for sulfur [20,41] which follows the principle of Hard-Soft-Acid-Base, it is quite believed that the SCN⁻ ions can be easily and selectively adsorbed on the surface of Au nanoparticles with a strong interfacial interaction of Au-S binding. In fact, for the CdS/Au-SCN photocatalysts, bi-directionally strong-coupling interfaces are formed as the Au nanoparticles can also be strongly adsorbed by lattice S²⁻ on CdS surface in addition to the SCN⁻ ions (Fig. 2B-c). Therefore, the CdS/Au-SCN photocatalysts with a strong-coupling interface can be easily prepared by the presence feasible and mild solution route.

3.2. Morphology and microstructures of CdS/Au-SCN photocatalysts

The controlled preparation of CdS/Au-SCN photocatalysts can first be demonstrated by FESEM, TEM and XRD results. Fig. 3(A–D) shows the FESEM images of the CdS, CdS/Au, CdS/Au-SCN(0.5 mM), and CdS/SCN samples. It can be found that the CdS sample (Fig. 3A) displays an aggregated morphology with a wide size range of 200–400 nm due to a simple precipitation–calcination method. The corresponding XRD result (Fig. 4a) suggests that all the diffraction peaks of the sample are indexed to be the hexagonal phase of CdS (JCPDS card No. 77-2306). After the CdS surface is modified with Au cocatalyst, the resulting CdS/Au (Fig. 3B) sample shows a similar morphology with the CdS sample owing to a limited amount of Au cocatalyst (Au/CdS = 3 wt%). However, on the basis of its corresponding EDX result (inset in Fig. 3B), it is found that the Au element with an amount of ca. 1.99% can be clearly detected in addition to the main Cd and S signals from the CdS. In addition, the XRD pattern of the CdS/Au photocatalyst

(Fig. 4b) clearly exhibits the Au diffraction peak at 38.34° (the inset in Fig. 4), strongly suggesting that Au nanoparticles have successfully been deposited on the CdS surface. As for the CdS/Au-SCN(0.5 mM) sample (Fig. 3C), no obvious morphology difference can be found compared with the CdS/Au sample. However, the new C and N signals corresponding to SCN⁻ can be obviously found in the EDX result (the inset in Fig. 3C), suggesting that the SCN⁻ ions have been homogeneously loaded on the CdS/Au surface. To further observe the morphology and phase structure of the CdS/Au-SCN(0.5 mM) particles, its corresponding TEM images are shown in Fig. 3E and F. It is clear that Au nanoparticles with a size of 50–100 nm (showed by red circle) are well deposited on the host CdS surface. For the CdS/SCN (Figs. 3D and 4f) photocatalyst, the sample also show similar particle morphology and crystal structure with the pure CdS owing to limited adsorbed amount of SCN⁻ ions. Therefore, the above results clearly demonstrated that the CdS/Au-SCN photocatalysts have been successfully prepared by the present facile strategy.

XPS technology can further provide information about the formation of CdS/Au-SCN photocatalyst. Fig. 5A shows the XPS survey spectra for various samples. It can be concluded that the main XPS peaks of Cd and S elements can mainly be ascribed to the CdS phase, while the O element is most likely from H₂O or –OH adsorbed on the photocatalyst surface during the aqueous-route preparation. Moreover, new XPS peaks of Au element are found in the CdS/Au (Fig. 5A-b) and CdS/Au-SCN (Fig. 5A-c and d) samples compared with pure CdS (Fig. 5A-a), suggesting the successful loading of Au cocatalyst. To obtain more detailed chemical information of elements in the samples, their corresponding high-resolution XPS spectra are shown in Fig. 5B–E. It is clear that the XPS Au 4f spectrum of CdS/Au (Fig. 5B-b) shows two individual peaks at ca. 83.6 and 87.2 eV, which can be assigned to metallic Au of 4f_{7/2} and 4f_{5/2} peaks [42], respectively. However, after surface modification by SCN⁻, the binding energy of Au in the CdS/Au-SCN samples (Fig. 5B-c and d) shifts to a higher position. Fig. 5C and D shows the high-resolution XPS spectra of S2p and Cd 3d, respectively. Compared with pure CdS with a binding energy of 161.85 eV for S 2p and 405.30 eV for Cd 3d_{5/2} (Fig. 5C and 5D), it can be clearly seen that the XPS peaks of S and Cd elements in CdS/Au sample shifts to a lower binding energy ($E(S\ 2p) = 161.40\text{ eV}$; $E(Cd\ 3d_{5/2}) = 404.85\text{ eV}$) owing to a strong-coupling interface between CdS surface and metallic Au via the possible S-Au chemical bond. However, for the CdS/Au-SCN samples, their binding energies shift to a larger value ($(E(S\ 2p) = 161.70\text{ eV})$; $E(Cd\ 3d_{5/2}) = 405.10\text{ eV}$) than those of CdS/Au, mainly

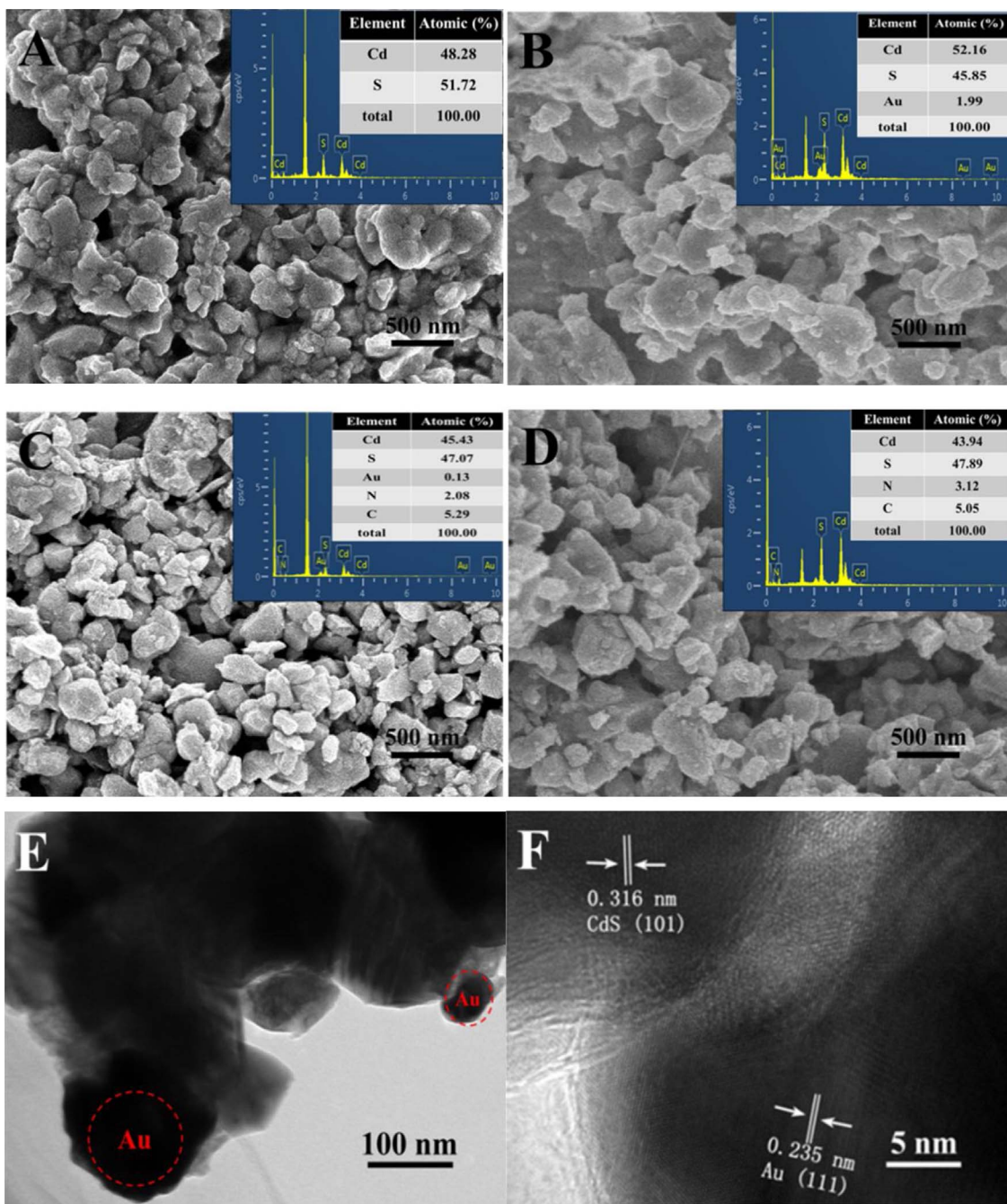


Fig. 3. FESEM/EDX of different samples: (A) CdS, (B) CdS/Au, (C) CdS/Au-SCN (0.5 mM), (D) CdS/SCN, and (E) TEM images of CdS/Au-SCN(0.5 mM).

due to the excellent selective adsorption of SCN^- on the Au surface. Fig. 5E shows the high-resolution XPS spectra of C1s for the CdS/Au before and after modification with SCN^- . Compared with the pure CdS (the XPS peak at ca. 284.6 eV is from the adventitious C element from XPS instrument itself), a new C peak at ca. 292.1 eV is clearly found in the resultant CdS/Au-SCN(0.5 mM) and CdS/Au-SCN(5 mM) samples, which can possibly be ascribed to the $\text{C}\equiv\text{N}$ in SCN^- . Moreover, its intensity enhances with the increase of SCN^- concentration, revealing that more SCN^- ions have been strongly adsorbed on the Au surface. Therefore, the above results clearly indicated that the SCN^- ions have been successfully and selectively loaded on the Au surface with a strong interfacial interaction, resulting in the formation of CdS/Au-SCN photocatalysts.

Fig. 6 shows the UV-vis spectra of CdS, CdS/Au, CdS/Au-SCN, and CdS/SCN samples. Pure CdS nanoparticles (Fig. 6a) usually exhibit a

strong and broad visible-light absorption in the region of 400–530 nm due to its small band gap (ca. 2.40 eV) [43]. After the Au cocatalyst is loaded on the CdS surface, the resultant CdS/Au photocatalyst (Fig. 6b) exhibits a significantly enhanced visible-light absorption in the range of 530–800 nm owing to the formation of Au nanoparticles on the CdS surface, in good agreement with its corresponding color change from yellow to brown (the inset of Fig. 6b). When the SCN^- is further modified on the CdS/Au surface to form CdS/Au-SCN photocatalyst (Fig. 6c–e), it is found that the visible-light absorption can be further improved and the corresponding samples show a deeper brown color (the inset of Fig. 6c–e), possibly due to the formation of a strong coupling interface between Au and SCN. However, different from CdS/Au and CdS/Au-SCN, CdS/SCN sample exhibits similar visible-light absorption to CdS with its corresponding color change from light yellow to deep yellow (the inset in Fig. 6f), which is clearly shown in the

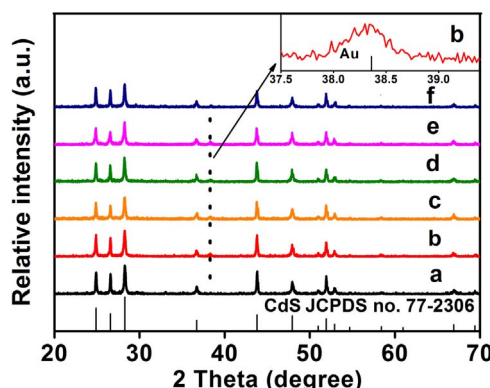


Fig. 4. XRD patterns of different samples: (a) CdS, (b) CdS/Au, (c) CdS/Au-SCN(0.1 mM), (d) CdS/Au-SCN(0.5 mM), (e) CdS/Au-SCN(5 mM), and (f) CdS/SCN.

similar UV-vis spectra.

The strong adsorption of SCN⁻ ions on the Au nanoparticles can also be well demonstrated by the following differential pulse voltamograms, as shown in Fig. 7. In this case, metallic Au was first loaded on the glassy carbon electrode (GCE) to prepare GCE/Au, and SCN⁻

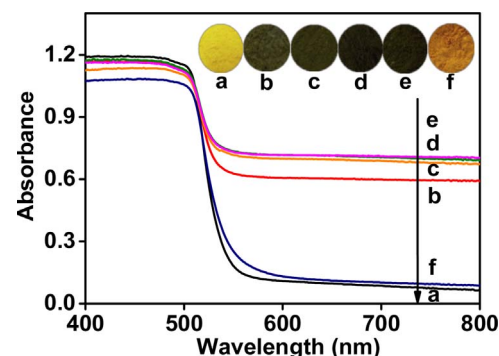


Fig. 6. UV-vis diffuse reflectance spectra of different samples: (a) CdS, (b) CdS/Au, (c) CdS/Au-SCN(0.1 mM), (d) CdS/Au-SCN(0.5 mM), (e) CdS/Au-SCN(5 mM), and (f) CdS/SCN.

ions were subsequently adsorbed on the metallic Au surface to form GCE/Au-SCN. For the GCE/Au, a high peak current corresponding to the electrochemical response of [Fe(CN)₆]^{3-/-4-} is obviously observed, suggesting that the Au nanoparticles possess excellent electrochemical properties to rapidly promote interfacial catalytic reaction. After the

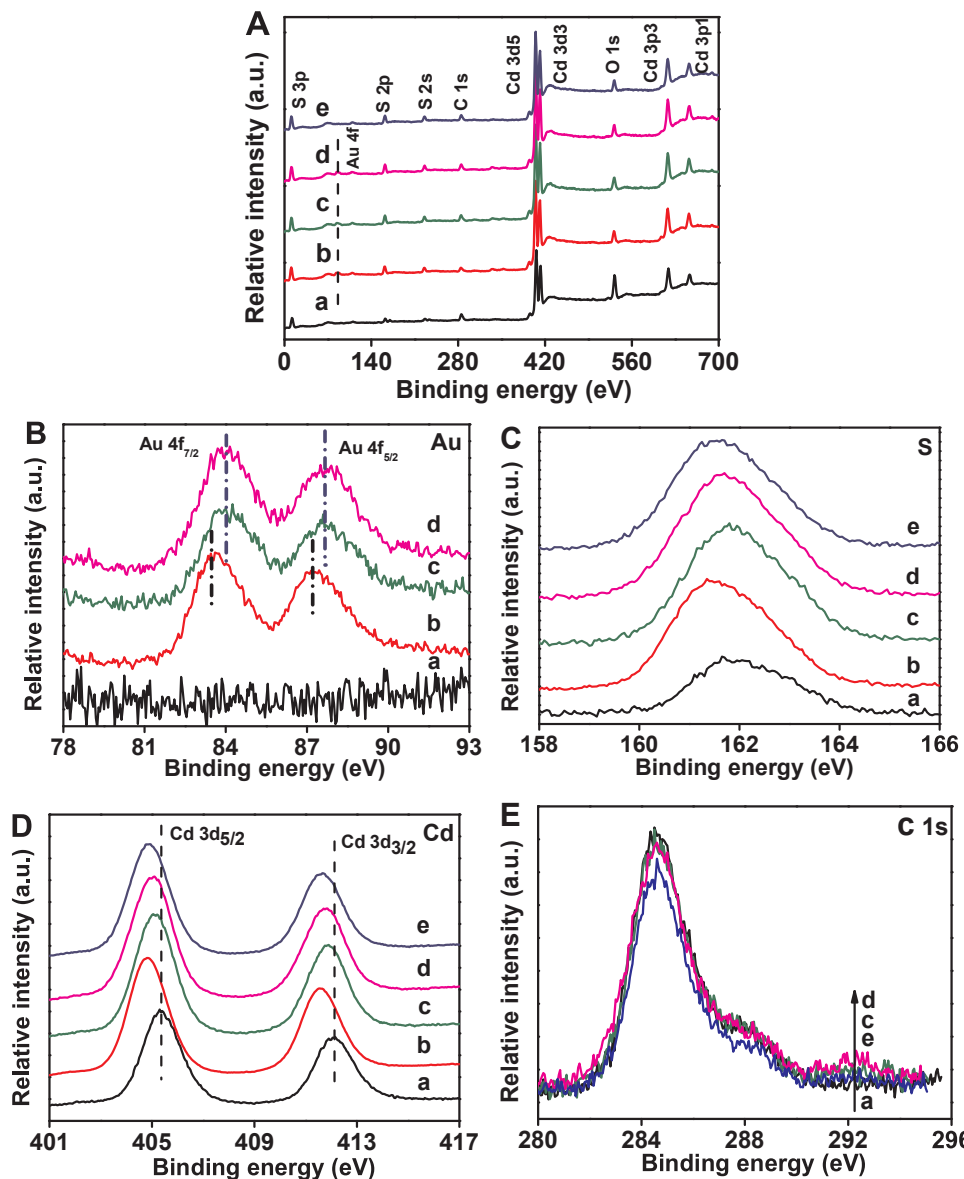


Fig. 5. (A) XPS survey spectra and (B-E) the high-resolution XPS spectra of (B) Au 4f, (C) S 2p, (D) Cd 3d, and (E) C 1s for various samples: (a) CdS, (b) CdS/Au, (c) CdS/Au-SCN(0.5 mM), (d) CdS/Au-SCN(5 mM), and (e) CdS/SCN.

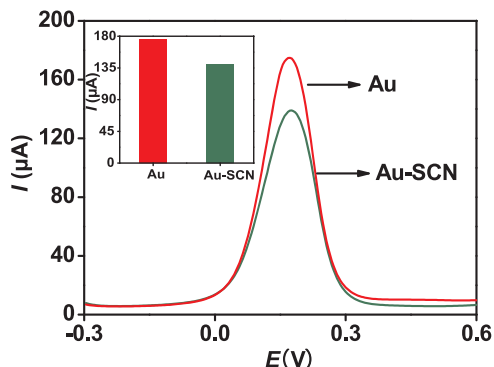


Fig. 7. Differential pulse voltammograms (DPV) of $[Fe(CN)_6]^{3-/4-}$ at Au/GCE before and after the SCN^- adsorption.

GCE/Au is adsorbed with SCN^- , a remarkably decreased current is observed, which can be ascribed to the fact that the SCN^- ions are strongly adsorbed on the Au surface, causing the weaker adsorption of negatively charged $[Fe(CN)_6]^{3-/4-}$ molecules and lower interfacial catalytic reactions. Therefore, it is clear that the SCN^- ions can be easily adsorbed on the Au nanoparticles with a strongly coupling interface.

3.3. Photocatalytic performance and mechanism

Photocatalytic H₂-evolution performances over various photocatalysts are evaluated under visible light ($\lambda \geq 420$ nm) irradiation, as shown in Fig. 8A. It can be seen that pure CdS exhibits an obvious H₂-evolution activity ($47.29 \mu\text{mol h}^{-1}$) with an apparent quantum efficiency (QE) of 4.85% due to its appropriate band gap (2.4 eV) [44] and strong reduction potential (-0.51 V vs. SHE) for H₂ evolution [8,45]. After surface deposition of Au nanoparticles, the resultant CdS/Au shows an improved H₂-evolution performance ($73.70 \mu\text{mol h}^{-1}$) with a

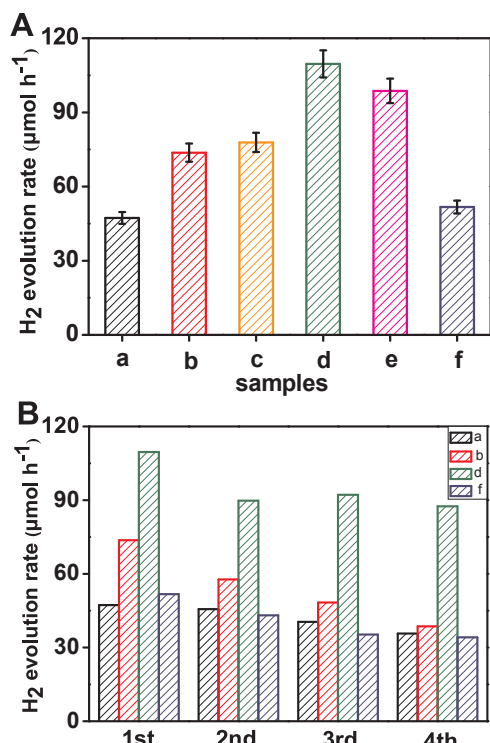


Fig. 8. (A) The photocatalytic H₂-evolution activity and (B) the repeating performance of different samples: (a) CdS, (b) CdS/Au, (c) CdS/Au-SCN(0.1 mM), (d) CdS/Au-SCN(0.5 mM), (e) CdS/Au-SCN(5 mM), and (f) CdS/SCN.

QE of 7.57% owing to the rapid transfer and separation of photo-generated electrons from CdS surface to Au nanoparticles. With the further selective adsorption of SCN^- on Au surface, all the CdS/Au-SCN samples display a further improved H₂-production performance. Especially, the resultant CdS/Au-SCN(0.5 mM) achieves the highest photocatalytic activity ($109.60 \mu\text{mol h}^{-1}$) with a QE of 11.25%, which is clearly higher than that of CdS and CdS/Au by a factor of 2.3 and 1.5 times, respectively. To further investigate the effect of K⁺ ions on the photocatalytic performance of CdS/Au, the NaSCN and KCl were also used as the precursors in addition to the KSCN, and the corresponding results were shown in Fig. S2. It is found that the H₂-production rate of the CdS/Au-NaSCN(0.5 mM) is comparable to that of CdS/Au-KSCN (0.5 mM), while the CdS/Au-KCl(0.5 mM) showed a negligible improvement of the photocatalytic performance compared with the CdS/Au. Therefore, it is quite believed that the counterion K⁺ has a negligible effect on the final photocatalytic activity of CdS/Au. To further evaluate their repeating H₂-production performance, cycling tests are performed under an identical condition and their corresponding results are shown in Fig. 8B. It is found that the CdS/Au-SCN photocatalyst still can maintain an obviously higher photocatalytic performance than the CdS, CdS/Au, and CdS/SCN photocatalysts during repeating tests.

The above results clearly indicate that the photocatalytic H₂-evolution of CdS/Au can be greatly improved after the selective adsorption of SCN^- on the Au surface. Thus, it is very interesting and worthwhile to investigate the potential photocatalytic mechanism of CdS/Au-SCN photocatalyst for the improved H₂-evolution performance. A possible photocatalytic mechanism of CdS/Au-SCN photocatalyst is shown in Fig. 9. For the CdS/Au-SCN photocatalyst, the unsaturated sulfur atoms in the negative SCN^- ions can effectively adsorb positive H⁺ ions from solution due to their strong nucleophilicity [46,47], while the SCN^- with a strong electron-withdrawing is essential to facilitate the interfacial electron transfer from Au surface [34] and subsequently promotes the direct reduction of protons to hydrogen by photo-excited electrons (Fig. 9A). Obviously, in the CdS/Au-SCN photocatalyst system, the Au nanoparticles first work as electron capturers (or electron sink) to rapidly capture photogenerated electrons from the conduction band of CdS (step (1)) and then function as electron-transfer mediator to steadily transports photogenerated electrons to the adsorbed SCN^- ions (step (2)), while the SCN^- ions serve as interfacial catalytic active-sites to effectively adsorb H⁺ ions from solution and then promote the following interfacial H₂-evolution reaction (step (3) in Fig. 9B). Hence, it is clear that the excellent synergistic effect between Au and SCN^- is account for the greatly improved photocatalytic H₂-evolution performance of CdS/Au-SCN photocatalyst.

To further confirm that the SCN^- can serve as the interfacial catalytic active-site to effectively adsorb H⁺ ions from solution and promote the rapid H₂-evolution reaction, the photoelectrocatalytic performances of the various samples were evaluated. Fig. 10A displays the typical polarization curves of blank CdS, CdS/Au, and CdS/Au-SCN (0.5 mM) samples. It can be seen that the loading of Au onto CdS obviously enhances the current density, indicating that Au functions as a cocatalyst to promote the reduction of H⁺ to H₂. With the further adsorption of SCN^- on Au surface, the CdS/Au-SCN(0.5 mM) sample displays a further improved current density, which can be attributed to the fact that the adsorbed SCN^- can serve as the interfacial catalytic active-site to effectively adsorb H⁺ ions from solution. Fig. 10B shows the transient photocurrent responses of the samples. It can be found that CdS/Au samples exhibits a higher transient photocurrent density than bare CdS. After adsorption of SCN^- ions, all the resultant CdS/Au-SCN photocatalysts display a further improved transient photocurrent density, strongly suggesting obviously enhanced separation efficiency of photogenerated charges and rapid interfacial H₂-evolution reactions by Au and SCN^- cocatalysts, in good agreement of the results in Fig. 8A. Fig. 10C shows the IPCE action spectra of the CdS/Au photocatalyst before and after selective adsorption of SCN^- . It is found that the IPCE curves of the CdS/Au and CdS/Au-SCN photocatalysts are

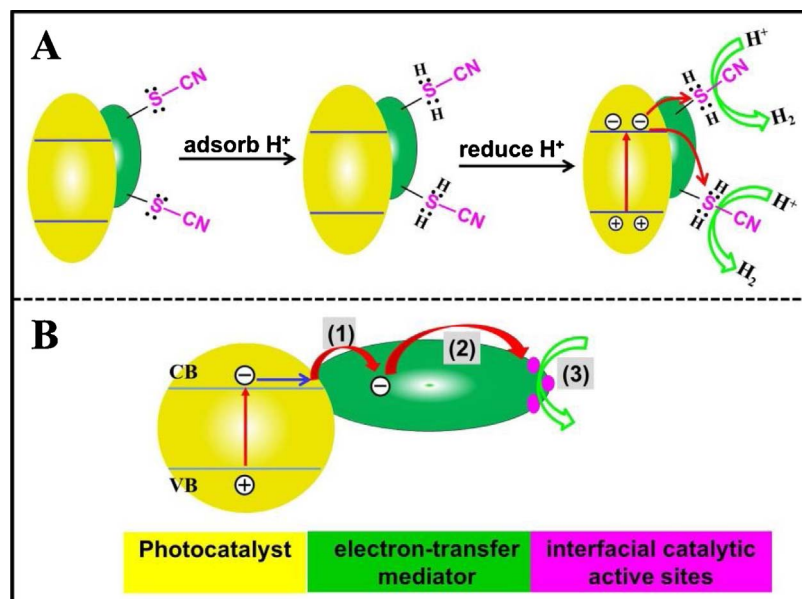


Fig. 9. (A) The photocatalytic H_2 -evolution progress of CdS/Au-SCN photocatalyst and (B) the general synergistic-effect mechanism of electron-transfer mediator and interfacial catalytic active site.

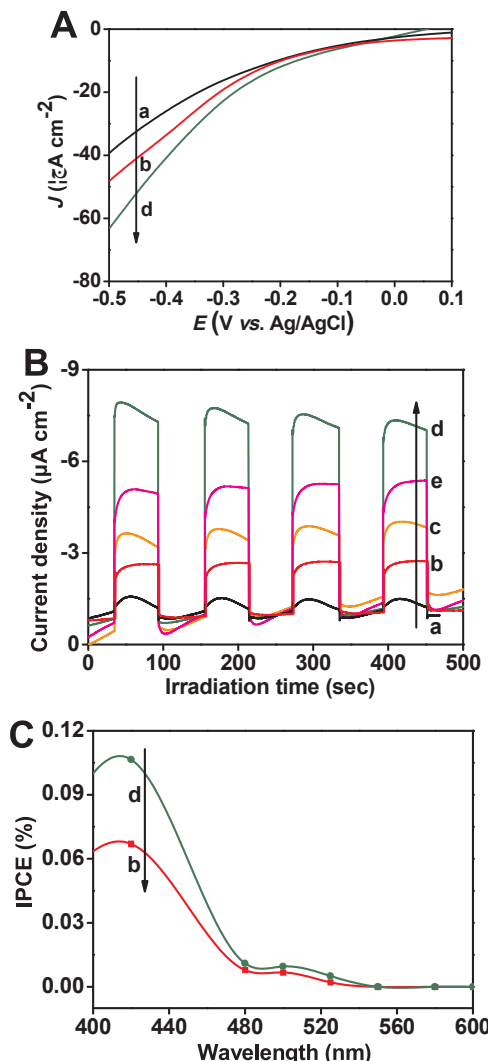


Fig. 10. (A) Linear sweep voltammetry (LSV) curves, (B) transient photocurrent response and (C) IPCE action spectra of different samples: (a) CdS, (b) CdS/Au, (c) CdS/Au-SCN (0.1 mM), (d) CdS/Au-SCN(0.5 mM), and (e) CdS/Au-SCN(5 mM).

consistent with their corresponding UV-vis diffuse reflectance spectra (Fig. 6), clearly suggesting that the photocatalytic H_2 -evolution performance of both the CdS/Au and CdS/Au-SCN can only be caused by the band-gap excitation of CdS semiconductor. In addition, compared with the CdS/Au, the CdS/Au-SCN obviously exhibits an improved IPCE in the range of 400–480 nm, strongly indicating the excellent synergistic effect of Au as an electron-transfer mediator and SCN^- as interfacial catalytic active site.

In addition to the CdS/Au-SCN system, the synergistic effect of electron-transfer mediator and interfacial catalytic active-site is a general and effective mechanism for the design and development of high-performance photocatalytic materials. To achieve this, the reasonable design and assembly of photocatalyst, electron-transfer mediator and interfacial reduction active sites are highly required to ensure the rapid transfer and separation of photogenerated electrons, and boost their following interfacial catalytic reactions for H_2 evolution or oxygen reduction (Fig. 9B). In this case, graphene nanosheets have been widely demonstrated to be an excellent electron-transfer mediator due to their large specific surface area and excellent electron transfer performance [48–50]. It is found that the large specific surface area of graphene can promote the homogeneous deposition and well dispersion for both of photocatalyst nanoparticles and interfacial catalytic active-sites, while its high electron mobility is favor of the rapid transportation of photogenerated electrons. As a consequence, various highly efficient graphene-based photocatalysts such as TiO₂-rGO-Fe(III) [31], MOF-rGO-MoS₂ [51], and TiO₂-rGO-Cu [28] have been widely developed. For the noble metal cocatalyst, although they also exhibit excellent electron capture and electron-transfer performance, the reports about noble metal as the electron-transfer mediator are still very limited owing to the absence of effective interfacial catalytic active-sites. Therefore, it is very necessary to develop new interfacial catalytic active-sites for the surface modification of noble metals to further improve the photocatalytic performance.

4. Conclusions

In summary, the SCN^- ions as the catalytic active sites have been selectively and successfully adsorbed on the Au surface of CdS/Au photocatalysts to prepare highly efficient CdS/Au-SCN photocatalysts by a facile impregnation method. Compared with the unmodified CdS and single-cocatalyst modified CdS photocatalysts (such as CdS/Au and CdS/SCN), the resultant CdS/Au-SCN photocatalysts exhibit an

obviously improved photocatalytic H₂-evolution activity. Especially, the CdS/Au-SCN(0.5 mM) reaches the highest photocatalytic activity (109.60 μmol h⁻¹) with a QE of 11.25%, which is clearly higher than that of CdS and CdS/Au by a factor of 2.3 and 1.5 times, respectively. On the basis of the experimental results, a synergistic effect mechanism of Au and SCN⁻ was proposed to account for its improved photocatalytic performance, namely, the Au nanoparticle functions as an effective electron-transfer mediator for the steady capture and rapid transportation of photogenerated electrons from CdS surface, while the adsorbed SCN⁻ serves as the interfacial catalytic active-site to effectively adsorb H⁺ ions from solution and promote their rapid interfacial H₂-evolution reaction. The present work will open up a novel strategy for the development of highly efficient photocatalytic materials for hydrogen production.

Acknowledgements

This work was supported by the National Natural Science Foundation of China (21477094, 51472192, and 51672203). This work was also financially supported by the Fundamental Research Funds for the Central Universities (WUT 2017IB002).

Appendix A. Supplementary data

Supplementary data associated with this article can be found, in the online version, at <http://dx.doi.org/10.1016/j.apcatb.2017.08.080>.

References

- [1] J. Ran, J. Zhang, J. Yu, M. Jaroniec, S.Z. Qiao, Chem. Soc. Rev. 43 (2014) 7787–7812.
- [2] Z.F. Huang, J. Song, K. Li, M. Tahir, Y.T. Wang, L. Pan, L. Wang, X. Zhang, J.J. Zou, J. Am. Chem. Soc. 138 (2016) 1359–1365.
- [3] S. Wang, Y. Zhang, T. Zhang, F. Dong, H. Huang, Appl. Catal. B: Environ. 208 (2017) 75–81.
- [4] N. Srinivasan, Y. Shiga, D. Atarashi, E. Sakai, M. Miyauchi, Appl. Catal. B: Environ. 179 (2015) 113–121.
- [5] H. Tong, S. Ouyang, Y. Bi, N. Umezawa, M. Oshikiri, J. Ye, Adv. Mater. 24 (2012) 229–251.
- [6] W.J. Jiang, Y.F. Zhu, G.X. Zhu, Z.J. Zhang, X.J. Chen, W.Q. Yao, J. Mater. Chem. A 5 (2017) 5661–5679.
- [7] K. Deng, L. Li, Adv. Mater. 26 (2014) 2619–2635.
- [8] X. Jia, M. Tahir, L. Pan, Z.F. Huang, X. Zhang, L. Wang, J.J. Zou, Appl. Catal. B: Environ. 198 (2016) 154–161.
- [9] H. Yu, F. Chen, F. Chen, X. Wang, Appl. Surf. Sci. 358 (2015) 385–392.
- [10] W. Jiang, Y. Liu, R. Zong, Z. Li, W. Yao, Y. Zhu, J. Mater. Chem. A 3 (2015) 18406–18412.
- [11] Y. Shi, H. Li, L. Wang, W. Shen, H. Chen, ACS Appl. Mater. Interfaces 4 (2012) 4800–4806.
- [12] C.C. Nascimento, G.R.S. Andrade, E.C. Neves, C.D.A.E.S. Barbosa, L.P. Costa, L.S. Barreto, I.F. Gimenez, J. Phys. Chem. C 116 (2012) 21992–22000.
- [13] K. Wu, H. Zhu, Z. Liu, W. Rodríguez-Córdoba, T. Lian, J. Am. Chem. Soc. 134 (2012) 10337–10340.
- [14] J. Jin, J. Yu, G. Liu, P.K. Wong, J. Mater. Chem. A 1 (2013) 10927–10934.
- [15] N. Zhang, S. Liu, X. Fu, Y.J. Xu, J. Mater. Chem. 22 (2012) 5042–5052.
- [16] M. Sathish, B. Viswanathan, R. Viswanath, Int. J. Hydrogen Energy 31 (2006) 891–898.
- [17] S. Min, G. Lu, J. Phys. Chem. C 116 (2012) 25415–25424.
- [18] T. Sreethawong, S. Yoshikawa, Catal. Commun. 6 (2005) 661–668.
- [19] A. Javey, J. Guo, Q. Wang, M. Lundstrom, H. Dai, Nature 424 (2003) 654–657.
- [20] P. Gomathisankar, D. Yamamoto, H. Katsumata, T. Suzuki, S. Kaneko, Int. J. Hydrogen Energy 38 (2013) 5517–5524.
- [21] M. Haruta, Catal. Today 36 (1997) 153–166.
- [22] A. Naldoni, M. D'Arienzo, M. Altomare, M. Marelli, R. Scotti, F. Morazzoni, E. Sell, V. Dal Santo, Appl. Catal. B: Environ. 130–131 (2013) 239–248.
- [23] J. Yang, D. Wang, H. Han, C. Li, Acc. Chem. Res. 46 (2013) 1900–1909.
- [24] Y. Xu, Y. Mo, J. Tian, P. Wang, H. Yu, J. Yu, Appl. Catal. B: Environ. 181 (2016) 810–817.
- [25] K. Chang, Z. Mei, T. Wang, Q. Kang, S. Ouyang, J. Ye, ACS Nano 8 (2014) 7078–7087.
- [26] Q.J. Xiang, F.Y. Cheng, D. Lang, ChemSusChem 9 (2016) 996–1002.
- [27] F. Dong, H. Wang, Z. Wu, J. Qiu, J. Colloid Interface Sci. 343 (2010) 200–208.
- [28] X.J. Lv, S.X. Zhou, C. Zhang, H.X. Chang, Y. Chen, W.F. Fu, J. Mater. Chem. 22 (2012) 18535–18541.
- [29] Q. Xiang, J. Yu, M. Jaroniec, J. Am. Chem. Soc. 134 (2012) 6575–6578.
- [30] T. Jia, A. Kolpin, C. Ma, R.C. Chan, W.M. Kwok, S.C. Tsang, Chem. Commun. 50 (2014) 1185–1188.
- [31] H. Yu, J. Tian, F. Chen, P. Wang, X. Wang, Sci. Rep. 5 (2015) 13083–13093.
- [32] H. Choi, W.T. Chen, P.V. Kamat, ACS Nano 6 (2012) 4418–4427.
- [33] A. Takai, P.V. Kamat, ACS Nano 5 (2011) 7369–7376.
- [34] Y. Choi, H.I. Kim, G.H. Moon, S. Jo, W. Choi, ACS Catal. 6 (2016) 821–828.
- [35] H. Yu, P. Xiao, P. Wang, J. Yu, Appl. Catal. B: Environ. 193 (2016) 217–225.
- [36] P. Wang, Y. Lu, X. Wang, H. Yu, Appl. Surf. Sci. 391 (2017) 259–266.
- [37] P. Chatchai, Y. Murakami, S.Y. Kishioka, A.Y. Nosaka, Y. Nosaka, Electrochim. Acta 54 (2009) 1147–1152.
- [38] L. Yang, X. Li, S. Yan, M. Wang, P. Liu, Y. Dong, C. Zhang, Anal. Methods 7 (2015) 5303–5310.
- [39] L. Yang, X. Li, Y. Xiong, X. Liu, X. Li, M. Wang, S. Yan, L.A.M. Alshahrani, P. Liu, C. Zhang, J. Electroanal. Chem. 731 (2014) 14–19.
- [40] H. Yu, X. Huang, P. Wang, J. Yu, J. Phys. Chem. C 120 (2016) 3722–3730.
- [41] J. Song, P.C. Huang, Y.Q. Wan, F.Y. Wu, Sens. Actuators B: Chem. 222 (2016) 790–796.
- [42] I. Majeed, M.A. Nadeem, M. Al-Oufi, M.A. Nadeem, G.I.N. Waterhouse, A. Badshah, J.B. Metson, H. Idriss, Appl. Catal. B: Environ. 182 (2016) 266–276.
- [43] S. Shen, L. Guo, X. Chen, F. Ren, S.S. Mao, Int. J. Hydrogen Energy 35 (2010) 7110–7115.
- [44] Q. Li, X. Li, S. Wageh, A.A. Al-Ghamdi, J. Yu, Adv. Energy Mater. 5 (2015) 1500010.
- [45] Z.G. Zhao, Z.F. Liu, M. Miyauchi, Adv. Funct. Mater. 20 (2010) 4162–4167.
- [46] R. Castarlenas, A. Di Giuseppe, J.J. Pérez-Torrente, L.A. Oro, Angew. Chem. Int. Ed. 52 (2013) 211–222.
- [47] Y. Liu, K. Ai, X. Cheng, L. Huo, L. Lu, Adv. Funct. Mater. 20 (2010) 951–956.
- [48] H. Yu, P. Xiao, J. Tian, F. Wang, J. Yu, ACS Appl. Mater. Interfaces 8 (2016) 29470–29477.
- [49] P. Wang, J. Wang, X. Wang, H. Yu, J. Yu, M. Lei, Y. Wang, Appl. Catal. B 132–133 (2013) 452–459.
- [50] S. Anandan, T. Narasinga Rao, M. Sathish, D. Rangappa, I. Honma, M. Miyauchi, ACS Appl. Mater. Interfaces 5 (2013) 207–212.
- [51] X. Hao, Z. Jin, H. Yang, G. Lu, Y. Bi, Appl. Catal. B: Environ. 210 (2017) 45–56.